RSC Advances

ROYAL SOCIETY
OF **CHEMISTRY**

www.rsc.org/advances

RSC Advances

RSCPublishing

PAPER

Oxidative and Membrane stress-mediated antibacterial activity of WS$_2$ and rGO-WS$_2$ Nanosheets

Govinda R. Navale,[1] Chandra Sekhar Rout,[2] Kushal N. Gohil,[3] Mahesh S. Dharne,[3*] Dattatray J. Late,[4*] Sandip S. Shinde[1*]

The graphene-based materials have strong cytotoxic attributes against bacteria due to their unique physico-chemical properties. We examine the antibacterial activity of graphene analogues tungsten disulphide (WS$_2$) and composite of reduced Graphene Oxide-tungsten disulphide(rGO-WS$_2$) nanosheets comparing with reduced Graphene Oxide (rGO) by time and concentration dependent viability assay and growth curve studies against four bacterial strains; Gram negative; *Escherichia coli* (*E. coli*), *Salmonella typhimurium* (*S. typhimurium*) and Gram positive; *Bacillus subtilis* (*B. subtilis*)*, Staphylococcus epidermidis* (*S. epidermidis*). The composite of rGO-WS$_2$ nanosheets caused significant bacterial growth retardation and inhibitory effect on the tested bacterial strains than WS$_2$ followed by rGO only. The tested *E. coli* and *B. subtilis* were more susceptible than the other strains. Mechanistic study reveals that the rGO and WS$_2$ did not produce superoxide anion ($O_2^{\bullet-}$) reactive oxygen species (ROS), but nanocomposite of rGO-WS$_2$ did produces both. However, all these materials did oxidize glutathione, which serves as redox state mediator in bacteria. We conclude that antimicrobial mechanism is due to combined effect of initial cell deposition on rGO-WS$_2$ materials, membrane stress due to direct contact with nanosheets, and the producing superoxide anion-independent oxidation mechanisms. Considering the beneficial aspects the physicochemical properties of rGO-WS$_2$ such as size, and conductivity, can be precisely customized to reduce their health and environmental risks factors.

1. Introduction

Graphene the 2D nanosheets of carbon atom has attracted wide interest due to its unusual electrical, magnetic and optical properties exhibited at single or few layers nanosheets.[1-6] This has attracted attention from the Physicist, Chemist, Material scientist and Biologist for a variety of fundamental phenomenon and new exciting applications. The zero bandgap of graphene hinders its wider application in various fields. The atomically thin two-dimensional metal dichalcogenides (TMDs) materials such as Molybdenum disulfide (MoS$_2$), Tungsten sulfide (WS$_2$), Molybdenum diselenide (MoSe$_2$), Tungsten diselenide (WSe$_2$), etc and their composite with graphene have been utilized as a graphene analogues material due to their semiconducting nature, tunable bandgap and optical properties.[7-17] The bulk WS$_2$ is a layered material with indirect bandgap of 1.3 eV whereas single layered WS$_2$ has a direct bandgap of 2eV. The reduced Graphene Oxide (rGO)[18-19] and

MoS$_2$[20] has been utilized for biological applications for antibacterial studies due to their intrinsic chemical, physical and optical properties[5,15] and also utilized widely for biomedical field for cell imaging and for DNA detection.[21-23] The electronic, magnetic, sensing, hydrogen evaluation, and photonic properties of rGO, few layered of WS$_2$ and its composite materials has been widely studied.[5,17,24-26] Recently, the 2D WS$_2$ nanosheets has found to used in medical diagnostics such as cancer therapy and drug delivery.[27-29] Compared to intensive study of biological effect of graphene and 2D MoS$_2$ sheets, there is absence of studies on possible toxicity effect of WS$_2$ and its composite with rGO materials, to realize the potential applications of pristine and composite nanosheets.

In the view of lack of studies on antibacterial activity of WS$_2$ and nanocomposite of rGO-WS$_2$ nanosheets, we considered it important to carry out the detail investigations on antibacterial activities of emerging 2D pristine WS$_2$ and

RSC Advances Accepted Manuscript

composite of rGO-WS$_2$ nanosheets. The composite nanosheets intensively inhibiting the growth activities of Gram negative *Escherichia coli* DH5α, *Salmonella typhimurium* and Gram positive *Bacillus subtilis*, *Staphylococcus epidermidis* bacterial cells.

In this article we are reporting for the first time 2D nanosheets WS$_2$ and its composite with rGO against *S. typhimurium* and *S. epidermidis* respectively, as both are well known pathogens to cause nosocomial infections.[30-31] The possibility of superoxide anion ($O_2^{\bullet-}$) induced reactive oxygen species (ROS) production was evaluated by the 2,3-Bis-(2-Methoxy-4-Nitro-5-Sulfophenyl)-2*H*-Tetrazolium-5-Carboxanilide (XTT) method. In vitro γ-L-glutamyl-L-cysteinyl-glycine (glutathione, GSH) oxidation was used to examine the superoxide anion independent oxidative stress. On the basis of these results, material characteristics related to their antibacterial activities were identified.

2. Experimental

2.1. Preparation of RGO, WS$_2$ and RGO-WS$_2$ Nanosheets:

A graphene oxide (GO) synthesis was performed using modified Hummer's method.[17] In the general synthesis process, concentrated H$_2$SO$_4$ (50 mL) was added to graphite powder (SP-1, Bay carbon), K$_2$S$_2$O$_8$ (1 g), and P$_2$O$_5$ (1 g) in a round-bottomed flask and heated at 80 °C. The obtained mixture was stirred using a magnetic stirrer and maintained at a temperature of 0°C in ice bath. Potassium permanganate (KMnO$_4$, 6g) was slowly added to the solution and stirred for 2h. The reaction was terminated by addition of excess amount of distilled water and 5 mL H$_2$O$_2$ solution. The mixture was filtered and washed with excess HCl. The resulting graphite oxide was suspended in distilled water again, followed by dialysis (Dialysis membrane: Spectrum Laboratories, MWCO-12-14,000) to remove excess HCl. The graphite oxide was exfoliated to give ~5 mg mL^{-1} GO solution by ultrasonication. After exfoliation, the solution was centrifuged at 3500 rpm for 10 min to remove the non-exfoliated graphite oxide and the top supernatant GO solution was used for hydrothermal reaction. Presence of oxygen functional groups makes the few-layered GO sheets highly hydrophilic and a stable dispersion was obtained.

The few layered WS$_2$ nanosheets were synthesized by a one-step hydrothermal reaction method as reported earlier.[9,17] In a typical experiment, 3 mM WCl$_6$ (Sigma-aldrich, 99.98%) and 15 mM thioacetamide (C$_2$H$_5$NS, Sigma-Aldrich, ≥99%) were dissolved in 40 mL DI water and stirred for 1h at room temperature by using a magnetic stirrer. The solution was then transferred to a 50 mL stainless steel autoclave, followed by heating at 265°C for 24 hours. After cooling the autoclave naturally, the as synthesized product was filtered, washed with DI water and then dried in the vacuum at 60°C for 6 hours.

The composite of WS$_2$-rGO nanosheets were prepared by the similar hydrothermal reaction condition as that for WS$_2$ sheets. The 8 mL of 5 mg mL^{-1} GO solution were added to the mixture of WCl$_6$ and thioacetamide and then the total

volume of the solution was maintained at 40 mL. Then similar procedure of WS$_2$ nanosheets synthesis was followed. During the hydrothermal synthesis process, the smaller size WS$_2$ nanosheets were found to be epitaxially formed on the GO and subsequently the GO were transformed into rGO.

2.2. Microbial strains, culture conditions and cell preparation

Four representative bacterial strains were selected for this study *E.coli* DH5α (dlacZ Delta M15 Delta (lacZYA-argF) U169 recA1 endA1 hsdR17(rK-mK+) supE44 thi-1 gyrA96 relA1 genotype; procured from Life technologies, USA), *S. typhimurium* NCIM 2501 (biofilm forming), *B. subtilis* NCIM 2063 and *S. epidermidis* NCIM 2493 (biofilm forming) were procured from National Collection of Industrial Microorganisms (NCIM) Pune, India. All strains were grown in Luria Bertani (LB) broth (Hi-Media, Mumbai) medium at 37 ºC, and harvested in the mid exponential growth phase as and when required. The cell culture was centrifuged at 6000 rpm for 10 min to collect cells, and cells were washed three times with isotonic saline solution to remove residual macromolecules and other growth medium constituents. The bacterial cell suspension was diluted in isotonic saline solution to obtain cell samples containing 10^7-10^8 colony forming units (CFU) mL^{-1} for antibacterial evaluations.

2.3. Bacterial cell growth

Bacterial growth kinetics was assayed as reported by Wang *et al.*,[32] with minor modifications. The 200 µL of the diluted cell suspensions of all four bacteria (10^7 to 10^8 CFU mL^{-1}) was mixed with 20 µL of five different concentrations of rGO, WS$_2$ and composite of rGO-WS$_2$ nanosheets (10, 50, 100 and 250 µg mL^{-1}) and incubated under shaking condition at 37°C for 2h with 150 rpm. A control sample contained 200 µL of the cell suspensions and 20 µL of saline water. The mixture was then transferred to 5 mL tubes, each containing 2 mL LB medium, and the tubes were inoculated on a rotary shaker at 150 rpm and 37 °C. The value of optical density (OD) at a wavelength of 620 nm was measured after every 2h on a Multiscan EX UV-VIS spectrometer (Thermo scientific, USA). Bacterial growth curves were generated by plotting OD$_{620nm}$ values versus time. All tests were prepared in triplicate.

2.4. Cell viability assessment

All three nanosheets were dispersed in nuclease free (NF) water with different concentrations of nanosheets (10, 50, 100, 250 µg mL^{-1}) for use. Dilutions ranging between 10^7-10^8 CFU mL^{-1} of *B. subtilis*, *E. coli* DH5α, *S. typhimurium* and *S. epidermidis* cells were incubated with dispersed in desired concentration of nanosheets in NF water at 37 ºC under 150 rpm shaking speed for time up to 6h. All bacterial samples in NF water without nanosheets were used as the control. The loss of viability of all the strains was evaluated by the time and concentration dependent viability (colony counting) method. Briefly, a series 10^{-4}, 10^{-5}, 10^{-6} cell dilutions (100 µL each) were spread onto LB plates after each 2h of time interval, and left to grow overnight (12-16 h) at 37 ºC. Colonies were

counted and compared with those on control plates to calculate total viable count (TVC) and percentage of non-viable cells. All tests were prepared in duplicate, and repeated at least on two separate occasions.

2.5. Cell morphology observation with TEM

The morphological changes of *S. epidermidis* bacteria (used as a model for TEM analysis) was further investigated using TEM after treatment with rGO,WS$_2$ and rGO-WS$_2$ nanosheets. The bacterial suspensions were treated with all three nanosheets for 2h at 37 ℃. After centrifugation at 3000 rpm for the bacterial cells were fixed with 2.5% glutaraldehyde for 30 min and washed with Phosphate buffer saline (pH 7.4). Subsequently, the samples were dehydrated in an ascending ethanol series (30, 50, 70, 80, 90 and 100%) for 15 min, respectively and dried in a vacuum oven. Finally diluted samples containing the bacterial cells were placed on the TEM grids and observed under TEM FEI TECNAI TF-30 (FEG) instrument.

2.6. Detection of Reactive Oxygen Species ($O_2{}^{\bullet-}$)

To find out the reactive oxygen species antibacterial paths, the possibility of superoxide radical anion ($O_2{}^{\bullet-}$) production was evaluated by measuring the absorption of XTT (2,3-bis (2-methoxy-4-nitro-5-sulfophenyl)-2H-tetrazolium-5-arboxanilide, Sigma Aldrich). XTT can be reduced by the superoxide radical anion ($O_2{}^{\bullet-}$) to form water-soluble XTT-formazan that has maximum absorption at 470 nm.[20,33] XTT (0.4 mM) with menadione (0.25 mM) was used as a positive control.The detailed protocol is described in the Supporting information.

2.7. Thiol Oxidation and Quantification

Following the method used in a previous study,[19-20] the concentration of thiols in GSH was quantified by the Ellmans assay.[36] rGO, WS$_2$ and composite of rGO-WS$_2$ (225 µL at 100 µg mL^{-1}) in 50mM bicarbonate buffer (pH 8.6) was added into 225 µL of GSH (0.8 mM in the bicarbonate buffer) to initiate oxidation. All samples were prepared in triplicate. The GSH or three nanosheets mixtures were transferred into a 24-well plate. The 24-well plate was covered with alumina foil to prevent illumination, and then placed in a shaker with a speed of 150 rpm at room temperature for incubation of 2h. After incubation, 785 µL of 0.05 M Tris-HCl and 15 µL of DNTB (Ellman's reagent, 5, 50-dithio-bis-(2-nitrobenzoic acid), Sigma-Aldrich) were added into the mixtures to yield a yellow product. All three was removed from the mixtures by filtration through a 0.22 µm syringe filters with membrane (Hi-media, India). 250 µL aliquot of filtered solutions from each sample was then placed in a 96-well plate. Their absorbance at 412 nm was measured on a Multiscan EX UV-VIS spectrometer (Thermo scientific, USA). GSH solution without graphene-based materials was used as a negative control. GSH (0.4 mM) oxidization by H$_2$O$_2$ (1 mM) was used as a positive control. The loss of GSH was calculated by the following formula: loss of GSH % = (absorbance of negative control - absorbance of sample)/absorbance of negative control x 100. After 2h incubation at the room temperature, 98% of GSH in the positive

control sample was lost, which is consistent with previous studies.[19,34]

3. Results and discussion

3.1.Antibacterial activity of rGO, WS$_2$, rGO-WS$_2$ nanosheets

Figure 1 shows a field emission scanning electron microscope (FE-SEM) image of rGO nanosheets (Fig 1a); few-layered WS$_2$ sheets (Fig 1b) and nanocomposite rGO-WS$_2$ (Fig 1c) nanosheets. The FE-SEM images shows that the WS$_2$ sheets is ~1–5 nm thick and their length is in the range of ~1–3 µm. The FE-SEM images of composite rGO-WS$_2$ exhibit a large number of 3D architect structure as compared to WS$_2$ and rGO sheets. [For more detail structural and morphological chartizations such as transimsiion electron microscopy (TEM), high-resulation transimssion electron microscopy (HRTEM), X-Ray diffraction (XRD), Energy-dispersive X-ray spectroscopy (EDAX), X-Ray Photoelectron spectsoscopy (XPS), Raman spectsocopy etc. please see the supporting information].

The antibacterial effect of rGO, WS$_2$ and rGO-WS$_2$ nanosheets against four bacterial strains including two Gram negative: *E. coli* DH5α (strain devoid of restriction-modification system, non pathogenic), *S. typhimurium* (pathogenic and bioflim forming) and two Gram positive: *B. subtilis, S. epidermidis* (pathogenic and bioflim forming) were used. Initially the growth kinetics study experiment was carried out using various concentrations of three nanosheets (0 (Control), 10, 50, 100 and 250 µg mL^{-1}), the death phase of all the bacteria (including pathogenic) at 250 µg mL^{-1} concentration were shown after 18h of incubation with WS$_2$ and rGO-WS$_2$ composite materials and low in rGO. These results shown that WS$_2$ and rGO-WS$_2$ nanosheets has better inhibitory effects on the growth kinetics towards the all tested bacterial strains than rGO nanosheets (see supporting information, Fig.S1).

Figure 2 shows the time and concentration dependent cell viability of all four bacterial strains with three nanosheets using same concentrations as mentioned above for 6h. The loss of viability (death rate) of bacterial cells was determined by the colony counting method, after every 2h interval (see materials and method).The figure 2 is summarizes in tabular form in Table 1, the comparative of viability loss percentage at highest concentration (250 µg mL^{-1}) for all nanosheets against four bacteria. It concluded that the bacterial cell loss viability steadily increases with concentration of rGO, WS$_2$ and rGO-WS$_2$ as well as incubation time. Among all the bacterial strains *S. epidermidis* was a more pathogenic which was used as a model orgamism for TEM analysis. The morphological changes of *S. epidermidis* after treating with three nanosheets were observed by TEM analysis (Figure 3) and optical microscopic images of disorted morphology of other strains of bacteria were shown in supporting information (see SI Fig S2). However, the tested nanosheets exhibited antibacterial activity in concentration and time dependent manner, and the composite

rGO-WS$_2$ nanosheets had a potentially better antibacterial activity than rGO and WS$_2$ nanosheets.

3.2. Antibacterial Mechanism of rGO, WS$_2$ and rGO-WS$_2$

Morphology and oxidative stress play important roles in the antibacterial activity of graphene[35-36] and other nanomaterials[36b], due to similarity in their structural and physicochemical properties of nanomaterials. Therefore, it is necessary to be thoroughly evaluating the possibility of cellular oxidative stress produced by rGO, WS$_2$ and composite of rGO-WS$_2$ nanosheets. It is evidenced that oxidative stress mediated by graphene based materials may arise from two paths, one is reactive oxygen species (ROS) mediated oxidative stress, in which oxidative stress mechanism is induced by ROS generated grapheme nanomaterials.[27] The second path is ROS-independent oxidative stress, in which nanomaterials may disrupt a specific microbial process by disturbing or oxidizing a vital cellular structure or component without ROS.[36] To evaluate the oxidative stress paths for rGO, WS$_2$ and rGO-WS$_2$, we initially measured the possibility of superoxide anion($O_2^{\bullet-}$) production using the XTT menadione mediated assay (See materials and methods) during incubation for 6h, results shown in Figure 4. The composite of rGO-WS$_2$ nanosheets have shown high ROS production compare to the rGO and WS$_2$ which has no significant absorption during 6h period. The XTT with menadione was used as a positive control to validate our XTT tests.[37] As compared to the absorbance of XTT along with these three nanosheets, the rGO-WS$_2$ composite enhanced the absorbance at 470 nm during the entire 6h incubation period. These results suggested that the composite materials could produce ROS. In contrast, the rGO and WS$_2$ nanomaterials mediate not significant absorbance detected. These results consistent with previous study of rGO, which shown low superoxide anion production due to single oxygen and hydroxyl radical derived from superoxide anions.[19,38] For reduction of XTT, rGO and WS$_2$ took more than 24 h (see supporting information Fig S3). We detected ROS produced by the rGO-WS$_2$ composite nanosheets in 2h of incubation and forming orange colour in 4h of dark incubation (see image S4 in SI). rGO-WS$_2$ composite nanosheets reduced XTT faster than menadione (a positive control). These results indicated the mechanism of nanomaterials could alter not only morphological but also the mechanistic property of antibacterial activity.

Further, we used in vitro GSH oxidation to examine the possibility of ROS-independent oxidative stress mediated by rGO, WS$_2$ and rGO-WS$_2$ nanocomposites by Ellmans assay[20,38] and results were summarized in Figure 5a and b; and in Table 2. In general, graphene based nanomaterials like rGO, GO, Gt, MoS$_2$ were known for GSH oxidation.[19-20] The GSH is an antioxidant to bacteria and fungi of plants, to examine the possibility of ROS-independent oxidative stress because it path play a significant role in the antimicrobial as well as toxic study of nanoparticles.[39]

Mechanistically GSH is a tri-peptide with HS-groups can be oxidized to form disulphide (–S–S–), converting GSH to glutathione disulphide. In bacteria, GSH concentration in the range from 0.1 to 10.0 mM preventing damages to cellular components.[40] GSH can prevent damages to cellular components caused by oxidative stress and it is oxidative stress indicator in cells.[41-42]

To evaluate the oxidation of GSH, was incubated with rGO, WS$_2$ and composite of rGO-WS$_2$, where in GSH (0.8 mM) in bicarbonate buffer (50.0 mM at pH 8.6) was used as negative control and H$_2$O$_2$ (1.0 mM) without three different nanosheets separately was used as a positive control in GSH oxidation experiment. The negative control suggests that our incubation conditions could not cause GSH oxidation. The oxidation capacity of the three nanosheets toward GSH was examine by taking absorbance at 412 nm.[19-20] As shown in Figure 5a, GSH oxidation by rGO, WS$_2$ and rGO was compared over a several concentrations 10, 50, 100 and 250 µg mL^{-1} for 2h, as concentration increases the glutathione oxidation also increases GSH oxidized after its exposure to 0, 50, 100 and 250 µg mL^{-1} concentrations of rGO was 18.6 ± 2.5 %, 76.4 ± 1.5 %, 88.2 ± 0.5 % and 97.2 ± 3.4 % respectively, and when exposure to WS$_2$ was 26.4± 1.4 %, 57.7± 2.6 %, 78.2± 3.5 % and 85.5± 1.5 % respectively, and finally exposure to composite of rGO-WS$_2$ nanosheets it was 34.3 ± 2.3 %, 79.2 ± 2.1 %, 98.2 ± 1.5 % and 99.3 ± 0.5 % respectively.

Among three types of graphene-based materials, rGO-WS$_2$ composite has the highest oxidation capacity toward GSH, followed by rGO and WS$_2$. When 0.8 mM GSH was incubated with 100 µg mL^{-1} of all these three nanosheets separately, the oxidation of GSH gradually increased with extending reaction time. Figure 4b shows the fraction of GSH oxidized by three nanosheets up to 6h of incubation.

Different oxidation capacities toward GSH among rGO, WS$_2$ and composite of rGO-WS$_2$ can be also attributed to their different electronic properties. The rGO, WS$_2$ and rGO-WS$_2$ representan electrical conductor, whereas graphene materials exhibit a zero-gap semiconductor with excellent electrical conductivity.[5,17] Conductivity of rGO is much higher than WS$_2$. Materials with higher conductivity, such as rGO and Graphite, they do not display higher oxidation capacities to GSH, compared with materials with lower conductivity, such as WS$_2$. Our observation suggests that rGO and rGO-WS$_2$ might share the similar mechanism as metallic SWCNTs.[34] They could act as a conductive bridge over the insulating lipid bi-layer to release cellular energy.[42] The oxidation capacities of the rGO, WS$_2$ and rGO-WS$_2$ of the nanosheets towards GSH have shown time and concentration dependent. Over all these results indicate that all three nanosheets are capable of inducing superoxide anion independent oxidative stress and can oxidize cellular components such asproteins and DNA, RNA materials.

Conclusions

The antibacterial activity of WS$_2$ and rGO-WS$_2$ composite nanosheets were evaluated by colony counting method and growth curve studies against four bacterial strains; Gram positive *B. subtilis* and *S. epidermidis*, Gram negative *E. coli* DH5α, and *S. typhimurium*. The composite of rGO-WS$_2$

nanosheets caused significant bacterial growth retardation and inhibitory effect on tested bacterial strains compare to WS_2. We demonstrated the detail mechanism of oxygen stress induced reactive oxygen species (ROS) effective with only rGO-WS_2, but in case GSH membrane mechanism stress shows with the all three nanosheets due to direct contact with nanosheets, and superoxide anion-independent oxidation. Results suggested that antimicrobial actions are contributed by both membrane and oxidation stress. We believe that the antimicrobial activity of WS_2-rGO composite nanosheets will be interesting in medical and pharmaceutical industrial applications.

Acknowledgements

Notes and references

[1]Organic Chemistry Division, CSIR-National Chemical Laboratory, Dr. Homi Bhabha Road, Pune 411008, Maharashtra, India. Email: ss.shinde@ncl.res.in

[2]School of Basic Sciences, Indian Institute of Technology Bhubaneswar, Bhubaneswar 751013, Odisha, India. Email: csrout@iitbbs.ac.in

[3]NCIM Resource Centre , CSIR-National Chemical Laboratory, Dr. Homi Bhabha Road, Pune 411008, Maharashtra, India. Email: ms.dharne@ncl.res.in

[4]Physical & Materials Chemistry Division, CSIR-National Chemical Laboratory, Dr. Homi Bhabha Road, Pune 411008, Maharashtra, India. Email: dj.late@ncl.res.in

† Electronic Supplementary Information (ESI) available: [Growth kinetics of four bacteria with different concentrations of three rGO, WS_2 and rGO-WS_2; optical microscopic images of the bacterial cells exposed to rGO, WS_2 and rGO-WS_2 nanosheets with 100 µg mL^{-1} concentrations for 2h; Superoxide radical anion production by XTT experiments for 24h by rGO, WS_2 and rGO-WS_2 nanosheets; ROS production by composite of RGO-WS_2 detected by monitoring color change]. The detail morphological and structural chartrization data such as TEM, HRTEM, X-RD, Raman spectsocopy, XPS, SEM and EDAX etc. Please See the DOI: 10.1039/b000000x/.

1   K. S. Novoselov, D. Jiang, F. Schedin, T. J. Booth, V. V. Khotkevich, S.V. Morozov, A. K. Geim, *Proc. Nat. Acad. Sci.* 2005, **102**, 10451.

2   K. S. Novoselov, A. K. Geim, S. V. Morozov, D. Jiang, Y. Zhang, S. V. Dubonos, I. V. Grigorieva, A. A. Firsov, *Science,* 2004, **306**, 666.

3   K. S. Novoselov, A. K. Geim, S. V. Morozov, D. Jiang, M. I. Katsnelson, I.V. Grigorieva, S.V. Dubonos, A. A. Firsov, *Nature,* 2005, **438**, 197.

4   (a) F. Schwierz, *Nat. Nanotech.*2010, **5**, 487. (b) D. J. Late, *Adv. Device Mater.* 2015,**1**,52.

5   A. Ghosh, D. J. Late, L. S. Panchakarla, A. Govindaraj, C. N. R. Rao, *J. Exp. Nanosci.* 2013, **4**, 313.

6   D. J. Late, U. Maitra, L. S. Panchakarla, U. V. Waghmare, C. N. R. Rao, *J. Phys.: Condens. Matter*, 2011, **23**, 055303.

7   B. Radisavljevic, A. Radenovic, J. Brivio, V. Giacometti, A. Kis, *Nature Nanotech.* 2011 **6**, 147.

8   D. J. Late, B. Liu, H. S. S. R. Matte, V. P. Dravid, C. N. R. Rao, *ACS Nano,*2012, **6**, 5635.

9   M. Thripuranthaka, R. V. Kashid, C. S. Rout, D. J. Late, *Appl. Phy. Lett.*2014, **104**, 081911.

10   H. S. S. R. Matte, A. Gomathi, A. K. Manna, D. J. Late, R. Datta, S. K. Pati, C. N. R. Rao, *Angue. Chem. Inter. Edit.* 2010, **49**, 4059.

11   D. J. Late, B. Liu, H. S. S. R. Matte, C. N. R. Rao, V. P. Dravid, *Adv. Fun. Mater.*2012, **22**, 1894.

12   (a) D. J. Late, P. A Shaikh, R. Khare, R. V. Kashid, M. Chaudhary, M. A More, S. B. Ogale, *ACS Appl. Mat. & Interfaces,* 2014, **6**, 15881. (b) D. Chakravarty, D. J. Late, Eur. J. Inorg. Chem. 2015, **11**, 1973. (c) D. Chakravarty, D. J. Late, *RSC Adv.* 5, 21700.

13   D. Jariwala, V. K. Sangwan, L. J. Lauhon, T. J. Marks, M. C. Hersam, *ACS Nano*, 2014, **8**, 1102.

14   (a) D. J. Late, Y. Huang, B. Liu, J. Luo, J. Acharya, S. N. Shirodkar, J. Luo, A. Yan, D. Charles, U. V. Waghmare, V. P. Dravid, C. N. R. Rao, *ACS Nano*, 2013, **7**, 4879. (b) P. K. Kannan, D. J. Late, H. Morgan, C. S. Rout, *Nanoscale*, 2015, DOI: 10.1039/C5NR03633J. (c) D. J. Late, C. S. Rout, *J. Nanomed. Res.* 2015, **2**, 00015.

15   M. Thripuranthaka, D. J. Late, *ACS Appl. Mat. & Interfaces,* 2013, **6**, 1158.

16   D. J. Late, S. N. Shirodkar, U. V. Waghmare,V. P. Dravid, C. N. R. Rao, *Chem. Phy. Chem,* 2014, 15, 1592.

17   C. S. Rout, P. D. Joshi, R.V. Kashid, D. S. Joag, M. A. More, A. J. Simbeck, M. Washington, S. K. Nayak, D. J. Late, *Scientific Reports,* 2013, **3**, 3282.

18   S. Liu, M. Hu, T. H. Zeng, R. Wu, R. Jiang, J. Wei, L. Wang, J. Kong, Y. Chen, *Langmuir,* 2012, **28**, 12364.

19   S. Liu, T. H. Zeng, M. Hofmann, E. Burcombe, J. Wei, R. Jiang, J. Kong, Y. Chen, *ACS Nano*, 2011, **5**, 6971.

20   X. Yang, J. Li, T. Liang, C. Ma, Y. Zhang, H. Chen, N. Hanagata, H. Su, M. Xu, *Nanoscale,* 2014, **6**, 10126.

21   L. Lin, Y. Xu, S. Zhang, I. M. Ross, A. C. M. Ong, D. A. Allwood, *ACS nano,*2013, **7**, 8214.

22   S. Wang, Y. Zhang, Y. Ning, G. J. Zhang, *Analyst,* 2015, **140**, 434.

23   B. Cai, S. Wang, L. Huang, Y. Ning, Z. Zhang, G. J. Zhang, *ACS Nano*, 2014, **8**, 2632.

24   Y. Ma, Y. Dai, M. Guo, C. Niu, J. Lu, B. Huang, *Chem. Phys.*, 2011, **13**, 15546.

25   M. A. Lukowski, A. S. Daniel, C. R. English, F. Meng, A. Forticaux, R. J. Hamersa, S. Jin, *Energy Environ. Sci.,* 2014, **7**, 2608.

26   M. Li , Q. Liu, Z. Jia, X. Xu , Y. Cheng, Y. Zheng, T. Xi, S. Wei, *Carbon*, 2014, **67**, 185.

27   Y. B. Zhang, S. F. Ali, E. Dervishi, Y. Xu, Z. R. Li, D. Casciano, A. S. Biris, *ACS Nano*, 2010, **4**, 3181.

28   Y. Yong, L. Zhou, Z. Gu, L. Yan, G. Tian, X. Zheng, X. Liu, X. Zhang, J. Shi, W. Cong, W. Yin, Y. Zhao, *Nanoscale,* 2014, **6**, 10394.

29   L. Cheng, J. Liu, X. Gu, H, Gong ,X. Shi, T. Liu, C. Wang, X. Wang, G. Liu, H. Xing, W. Bu, B. Sun, Z. Liu, *Adv. Mater.* 2014, **26**, 1886.

30   M. otto., *Nat. rev. Microbiol.* 2009, 7, 555.

31 J. Borecka, M. Hocmannova, W. J. van Leeuwen. *Zentralbl. Bakteriol. Orig. A.* 1976, 236, 262.

32 X. P. Wang, X. Q. Liu, H. Y. Han*, Colloids Surf., B,* 2013, **103**, 136.

33 H. Ukeda, S. Maeda, T. Ishii, M. Sawamura, Anal. Biochem. 1997, **251**, 206–209.

34 C. D. Vecitis, K. R. Zodrow, S. Kang and M. Elimelech, *ACS Nano*, 2010, **4**, 5471.

35 (a) D. Y. Lyon, P.P.J. Alvarez, *Environ. Sci. Technol*. 2008, **42**, 8127. (b) D. Y. Lyon, L. Brunet, G. W. Hinkal, M. R. Wiesner and P. J. J. Alvarez, *Nano Lett.,* 2008, **8**, 1539.

36 G. R. Navale, M. Thripuranthaka, D. J. Late, S. S. Shinde, *JSM Nanotechnol Nanomed,* 2015, *3*, 1033.

37 J. Meletiadis, J. W. Mouton, J. F. G. M. Meis, B. A. Bouman, J. P. Donnelly, P. E. Verweij, E. Network, *J. Clin. Microbiol*., 2001, 3402.

38 G. L. Ellman, Tissue sulfhydryl groups, Arch Biochem Biophys. 1959, **82**, 70.

39 A. Pompella, A. Visvikis, A. Paolicchi, V. De Tata, A. F. Casini, Biochem. Pharmacol. 2003, **66**, 1499.

40 R.C. Fahey, W. C. Brown, W. B. Adams, M. B.Worsham. J. Bacteriol., 1978. **133**, 1126.

41 A. Joshi, S. Punyani, S. S. Bale, H. C. Yang, T. Borca-Tasciuc, R. S. Kane, Nat. Nanotechnol. 2008, **3**, 41.

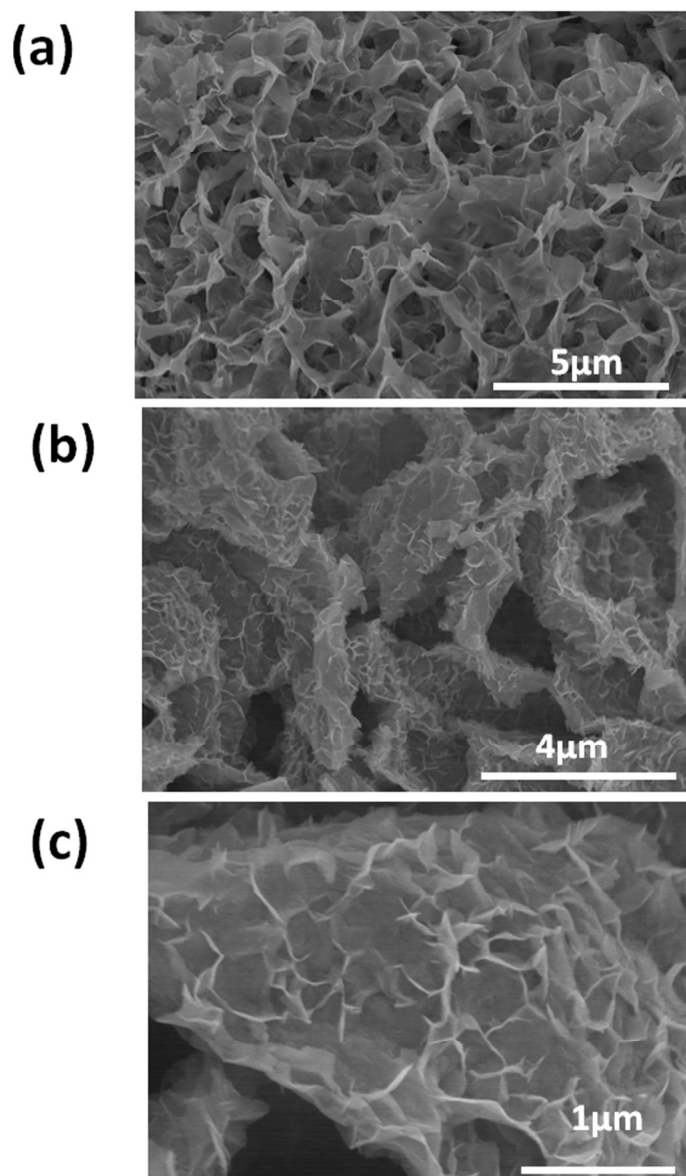42 O. Carmel-Harel, G. Storz, Annu. Rev. Microbiol. 2000, **54**, 439–461.

Figure 1:

Figure 1: FESEM image of (a) rGO, (b) WS$_2$ and (c) nanocompsoite of rGO-WS$_2$ nanosheets.

Figure 2:
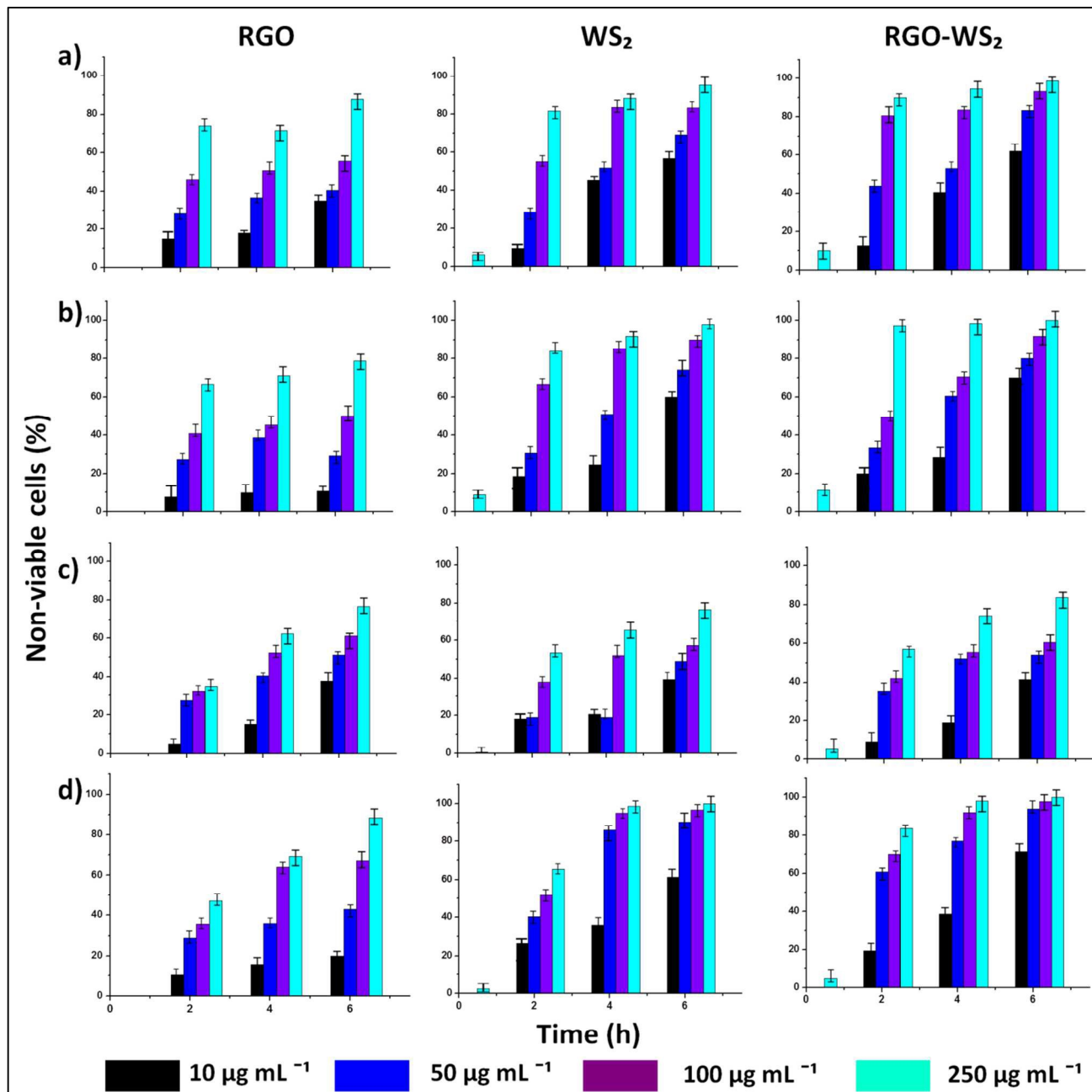

Figure 2: The loss of viability of a) *E.coli DH5a,* b) *S. typhimurium* (NCIM 2501),c) *B. subtilis* (NCIM 2063) and d) *S. epidermidis* (NCIM 2463) cells after incubation with 0 (Control), 10, 50, 100 and 250 µg mL^{-1}concentration of rGO, WS$_2$ and rGO-WS$_2$ nanosheets for different time exposure (0, 2, 4 and 6 h). The error bars represent the standard deviation.
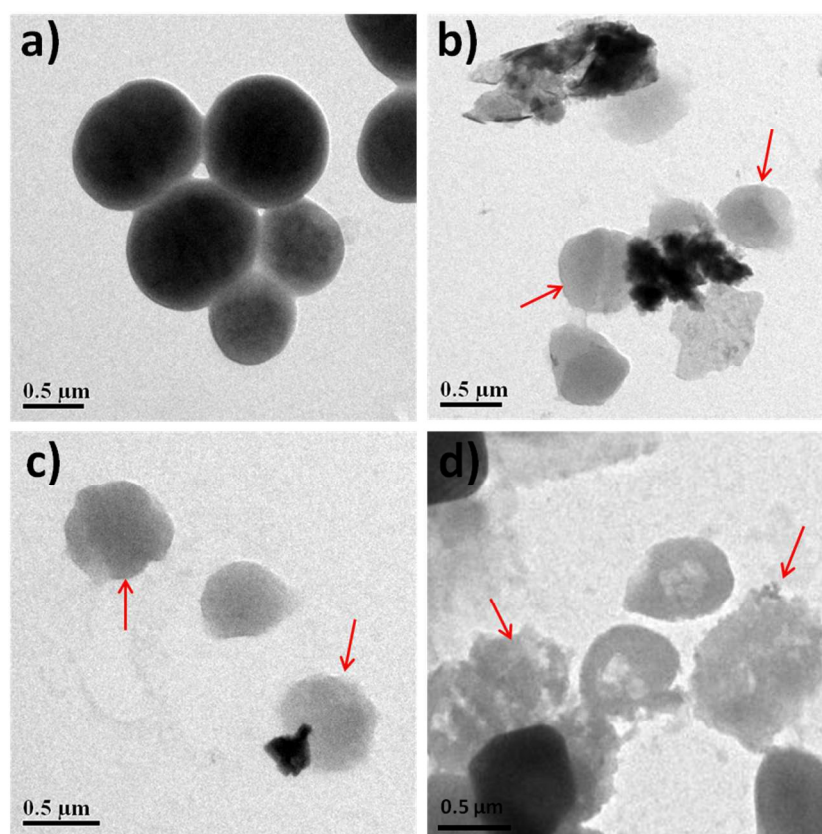
Figure 3:

Figure 3 : TEM images of (a) *S.epidermidis* control (without nanosheets); treated with 100 µg mL^{-1} of rGO (b); WS$_2$ (c) and composite of rGO-WS$_2$ nanosheets (d) after incubation for 2 h. Distorted morphology of bacteria indicated by red arrows.
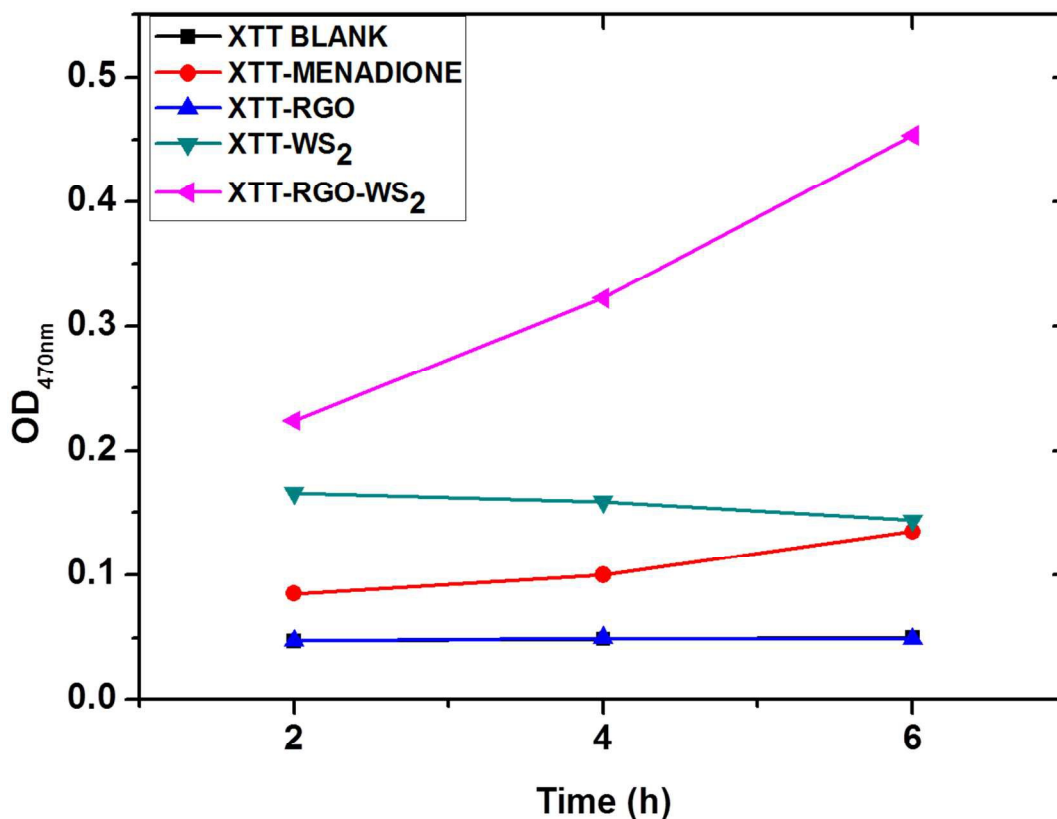
Figure 4:

Figure 4 : Production of superoxide radical anion ($O_2^{\bullet-}$) by rGO, WS_2 and rGO-WS_2 nanosheets. The dispersion concentration of the all three nanosheets was 100 mg mL^{-1}. The ($O_2^{\bullet-}$) production was monitored during the incubation of XTT (0.4 mM) with the rGO, WS_2 and rGO-WS_2 nanosheets at pH 7.0 in the dark for 6 h. Incubation of XTT with Menadione was performed as a positive control. XTT was used as a negative control.
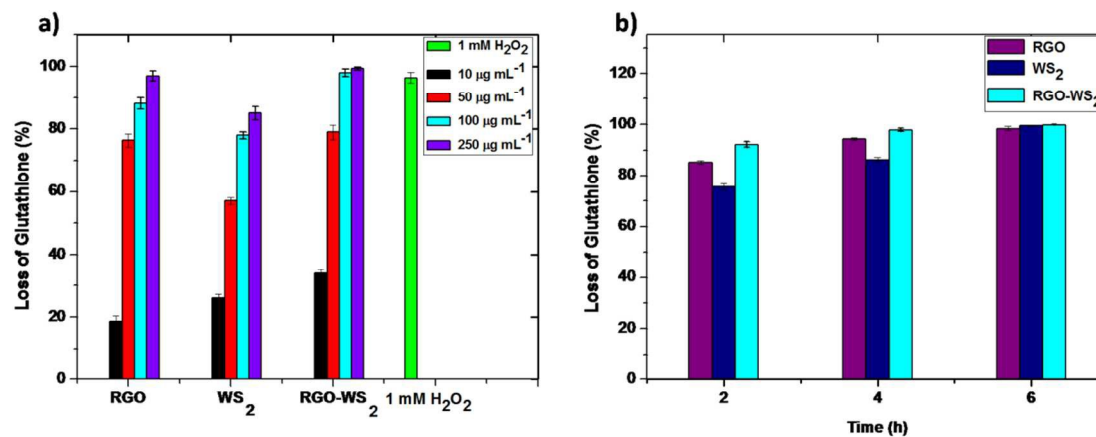
Figure 5:

Figure 5: a) Concentration dependent GSH (0.8mM) oxidation by rGO, WS$_2$ and rGO-WS$_2$ (at 10, 50, 100 and 250 µg mL^{-1}) H$_2$O$_2$ (positive control) after incubation for 2 h. b) Time dependent GSH (0.8mM) oxidation by rGO, WS$_2$ and rGO-WS$_2$ (at 100 µg mL^{-1}) after incubation for 2h, 4h and 6h.The error bars represent the standard deviation.

Table 1:

Table 1. The comparison of loss of viability (%) of four bacteria with respect to 250 µg mL^{-1} of rGO, WS$_2$ and rGO-WS$_2$ nanosheets at different time of interval. The standard deviation error was 0.5 ± 6.5.

Nanosheets ⟍ Bacteria	Loss of Glutathione[a] (%)					
	rGO		WS$_2$		rGO-WS$_2$	
	2 h	6 h	2 h	6 h	2 h	6 h
E. coli	64.23	87.7	81.88	96.67	90.22	98.67
S. typhimurium	35.12	62.5	53.43	76.54	57.05	83.89
B. subtilis	66.67	78.58	84.02	97.11	97.34	99.98
S. epidermidis	47.13	88.58	65.51	99.97	83.44	99.97

[a]Data extracted from figure 1.

RSC Advances Accepted Manuscript

Table 2:

Table 2. The Comparison among GSH oxidation at different time interval[a]

Time (h)	Loss of Glutathione (%)		
	rGO	WS$_2$	RGO-WS$_2$
2	85.1	75.4	92.2
4	94.3	86.3	97.8
6	98.3	99.5	99.8

[a]Data extracted from figure 3b.The standard deviation error was 0.2 ± 6.5.